

149906114

CONF. PAPER
N-117

LOCAL DATA INTEGRATION IN EAST CENTRAL FLORIDA

Jonathan L. Case* and John T. Manobianco
 NASA Kennedy Space Center / Applied Meteorology Unit / ENSCO, Inc.
 1980 N. Atlantic Ave. Suite 230
 Cocoa Beach, FL 32931

1. INTRODUCTION

The Applied Meteorology Unit has configured a Local Data Integration System (LDIS) for east central Florida which assimilates in-situ and remotely-sensed observational data into a series of high-resolution gridded analyses. The ultimate goal for running LDIS is to generate products that may enhance weather nowcasts and short-range (< 6 h) forecasts issued in support of the 45th Weather Squadron (45 WS), Spaceflight Meteorology Group (SMG), and the Melbourne National Weather Service (NWS MLB) operational requirements.

LDIS has the potential to provide added value for nowcasts and short-term forecasts for two reasons. First, it incorporates all data operationally available in east central Florida. Second, it is run at finer spatial and temporal resolutions than current national-scale operational models such as the Rapid Update Cycle (RUC; Benjamin et al. 1998) and Eta models. LDIS combines all available data to produce grid analyses of primary variables (wind, temperature, etc.) at specified temporal and spatial resolutions. These analyses of primary variables can be used to compute diagnostic quantities such as vorticity and divergence.

This paper demonstrates the utility of LDIS over east central Florida for a warm season case study. The evolution of a significant thunderstorm outflow boundary is depicted through horizontal and vertical cross section plots of wind speed, divergence, and circulation. In combination with a suitable visualization tool, LDIS may provide users with a more complete and comprehensive understanding of evolving mesoscale weather than could be developed by individually examining the disparate data sets over the same area and time.

2. DATA COVERAGE AND RESOLUTION

The utility of LDIS depends to a large extent on the reliability and availability of both in-situ and remotely-sensed observational data. Therefore, it is important to document all existing meteorological data sources around central Florida that can be incorporated by LDIS.

Data density and coverage in east central Florida vary considerably depending on the level in the atmosphere and distance from KSC/CCAS. The data that are currently incorporated into LDIS include surface, buoy, ship, Kennedy Space Center/Cape Canaveral Air Station (KSC/CCAS) tower and wind profiler, GOES-8, WSR-88D, rawinsonde, and commercial aircraft observations. The data sources that contain the finest horizontal resolution are WSR-88D (< 1 km), GOES-8 visible and infrared imagery (1 km and

4 km), and KSC/CCAS tower observations (4 km). The greatest frequency of observations are provided by WSR-88D, KSC/CCAS towers, profilers, ACARS (Aeronautical Radio, Inc. [ARINC] Communications, Addressing, and Reporting System), and GOES-8 satellite imagery (≤ 15 minutes). The largest variability in horizontal/vertical coverage and density occurs with aircraft data, satellite soundings, and satellite-derived winds. The maximum density of near-surface wind and temperature observations occurs within KSC/CCAS as a result of the tower network. Manobianco and Nutter (1998) provide further details on the data distribution, coverage, and resolution used for this specific configuration of LDIS.

3. ANALYSIS CONFIGURATION

The software utilized for LDIS is the Advanced Regional Prediction System (ARPS) Data Analysis System (ADAS; Brewster 1996; Carr et al. 1996) available from the University of Oklahoma. The analyses in ADAS are produced following Bratseth (1986) who developed an iterative Successive Corrections Method (SCM; Berghorsson and Doos 1955) that converges to statistical or optimum interpolation (OI). In general, OI schemes are superior to SCM methods because they can account for variations in data density, errors in the data, and dynamical relationships between variables such as the wind components and pressure.

The configuration of ADAS follows the layout used for the terminal wind analysis in the Integrated Terminal Weather System (ITWS; Cole and Wilson 1995). ADAS is run every 15 minutes at 0, 15, 30, and 45 minutes past the hour, over outer and inner grids with horizontal resolutions of 10 km and 2 km, respectively. The 10-km (2-km) analysis domain covers an area of 500 \times 500 km (200 \times 200 km) and consists of 30 vertical levels that extend from the surface to about 16.5 km above ground level. The vertical levels are stretched, with the finest resolution near the surface (20 m spacing) and the coarsest resolution at upper levels (~1.8 km spacing).

The background fields used on the 10-km analysis domain are the RUC grids of temperature, wind, relative humidity, and geopotential height at 25-mb intervals from 1000 to 100 mb. The RUC analyses are available at a horizontal resolution of 60-km every 3-h for the case study presented in this paper. The RUC grids are linearly interpolated in time every 15 minutes for each 10-km ADAS cycle. The resulting 10-km analysis grids are then used as background fields for analyses on the 2-km domain. This nested-grid configuration and cascade-of-scales analysis follows that used for terminal winds in ITWS. With such an approach, it is possible to analyze for different temporal and spatial scales of weather phenomena.

The observational data are incorporated into ADAS using multiple passes of the Bratseth scheme to account for the varying spatial resolution of the data sources. Five

*Corresponding author address: Jonathan Case, ENSCO, Inc., 1980 N. Atlantic Ave., Suite 230, Cocoa Beach, FL 32931. E-mail: jonc@fl.ensco.com.

computational passes are used for the 10-km grid and four passes are utilized on the 2-km grid. Data with similar resolutions are grouped together in the same computational pass such that ADAS incorporates each data source without excessively smoothing the resolvable meteorological features. This methodology ensures that each data source is utilized in ADAS to its maximum potential based on the meteorological features that the data can resolve.

4. DIAGNOSIS OF AN OUTFLOW BOUNDARY

A warm season case was selected from 26-27 July 1997 in order to investigate the capabilities and utility provided by ADAS. Both 10-km and 2-km grid analyses were generated for the warm season case at 15-minute intervals from 1800 UTC 26 July to 0200 UTC 27 July using all available data. However, only results from the 2-km analysis grid are presented in this section.

A typical, undisturbed warm season environment characterized the 26-27 July 1997 case. Early in the afternoon, scattered thunderstorms developed across the peninsula and a sea-breeze boundary was evident along the east coast (not shown). By 2212 UTC, strong thunderstorms developed southwest of KSC/CCAS and generated an outflow boundary that propagated northeastward as indicated by the Melbourne WSR-88D level II base reflectivity (Fig. 1a). The leading edge of the outflow boundary intersected the eastern tip of KSC/CCAS by 2242 UTC as shown in Figure 1b (counties and location of KSC/CCAS are given in Fig. 2a). This outflow boundary caused wind gusts greater than 15 m s^{-1} as noted on the KSC/CCAS mesonet towers around 2245 UTC (not shown). This case was chosen because the strong winds associated with the outflow boundary forced Atlas launch operation A1393 to be scrubbed for the day.

Using the fine-scale results of the 2-km ADAS analyses, the evolution of the wind speeds and wind vectors at 480 m (Figs. 2a-d) illustrates the formation and intensification of the outflow boundary during the late afternoon of 26 July. Wind speeds greater than 8 m s^{-1} develop over the Brevard/Osceola county border at 2215 UTC 26 July (Fig. 2a) and spread radially over the next 45 minutes. The maximum winds ($> 12 \text{ m s}^{-1}$) move northeastward into KSC/CCAS and offshore regions of central Brevard county by 2245 UTC (Fig. 3c), the approximate time that the Atlas launch was postponed.

Examination of level II radar reflectivity (Fig. 1) and radial velocity data (not shown) indicates that features present in the high-resolution wind analyses (Fig. 2) are consistent with the scale and motion of patterns associated with the observed thunderstorm. It should be noted that the detailed structure of horizontal winds associated with this outflow boundary would likely be easier to visualize in real-time using ADAS rather than WSR-88D radial velocity displays alone.

The evolution of the thunderstorm outflow can also be examined through the divergence of the horizontal wind on the 2-km ADAS grid. In Figure 3, plots of convergence (shaded), divergence (dashed lines), and horizontal winds are shown at 650 m for the same times as in Figure 2. At 2215 UTC, an area of low-level convergence is found over much of central Brevard county (Fig. 3a). Weak divergence is also found over northeastern Osceola county at this time. Fifteen minutes later, an extensive area of low-level divergence develops in southern Brevard county, behind the developing outflow boundary (Fig. 3b). Convergence along the outflow boundary spreads outward into central Brevard county (just south of KSC/CCAS), offshore of southern Brevard county, and into Indian River county. Divergence continues to intensify across much of interior Brevard county over the next 30 minutes beneath the dissipating thunderstorm (Figs. 3c and d), while the band of convergence spreads out radially along the leading edge of the outflow boundary.

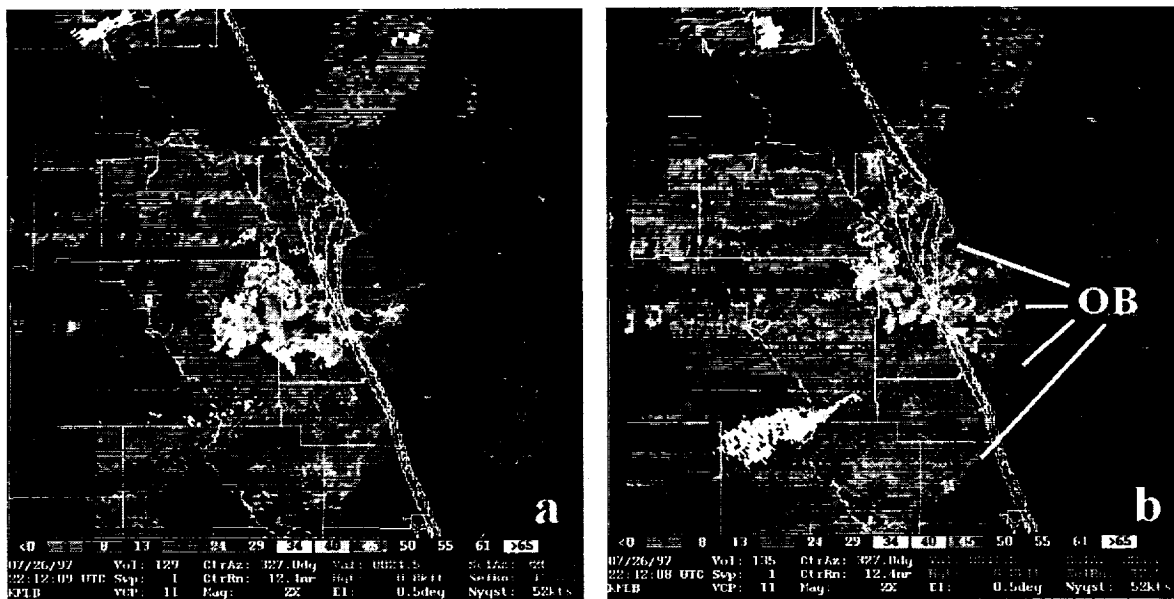


Figure 1. Base reflectivity images are shown from the Melbourne WSR-88D on 26 July at a) 2212 UTC and b) 2242 UTC. The leading edge of the outflow boundary is indicated by "OB" in panel b).

By 2300 UTC, a well-defined band of convergence arcs from northern Osceola county, across eastern Orange and northern Brevard county, into the offshore waters of Brevard county, and then back onshore in Indian River county (Fig. 3d). Strong divergence exceeding $8 \times 10^{-4} \text{ s}^{-1}$ occurs over east-central Brevard county.

The vertical structure of the convection is indicated by north-south cross sections of divergence and the vertical velocity (w) field through the developing thunderstorm outflow (Fig. 4 and 5 respectively). According to Brewster (1996), w is derived within ADAS from the analyzed horizontal winds (via continuity) and a constraint that the wind velocity normal to the bottom and top boundaries is zero. Deviations from these boundary conditions are treated as errors in the horizontal divergence that vary linearly with height. The w field is adjusted once these errors are removed and the horizontal wind field is relaxed such that total mass divergence domain-wide is zero.

A deep column of convergence is prevalent at 2215 UTC (Fig. 4a) associated with the strong convection southwest of

KSC/CCAS (Fig. 1a). The onset of the dissipating stage of the convection occurs at 2230 UTC when convergence transitions to divergence in the lowest 1000 m directly beneath the deep layer of maximum convergence (Fig. 4b). The leading edge of the outflow boundary is evident in Figure 4b given by the low-level convergence below 1000 m on either side of the newly-developed low-level divergence.

By 2245 UTC, the area of low-level divergence expands laterally and upward to 3000 m (Fig. 4c). The leading edge of the outflow boundary spreads rapidly north and southward (left and right, primarily below 1000 m) on either side of the intensifying low-level divergence maximum. Meanwhile, mid-level convergence remains strong, exceeding $-6 \times 10^{-4} \text{ s}^{-1}$ in the 3500–5500-m layer. By 2300 UTC, a well-developed signature exists for a downburst-producing thunderstorm (Fig. 4d). Strong mid-level convergence in the 3000–6000-m layer overlies a maximum in low-level divergence which exceeds $8 \times 10^{-4} \text{ s}^{-1}$.

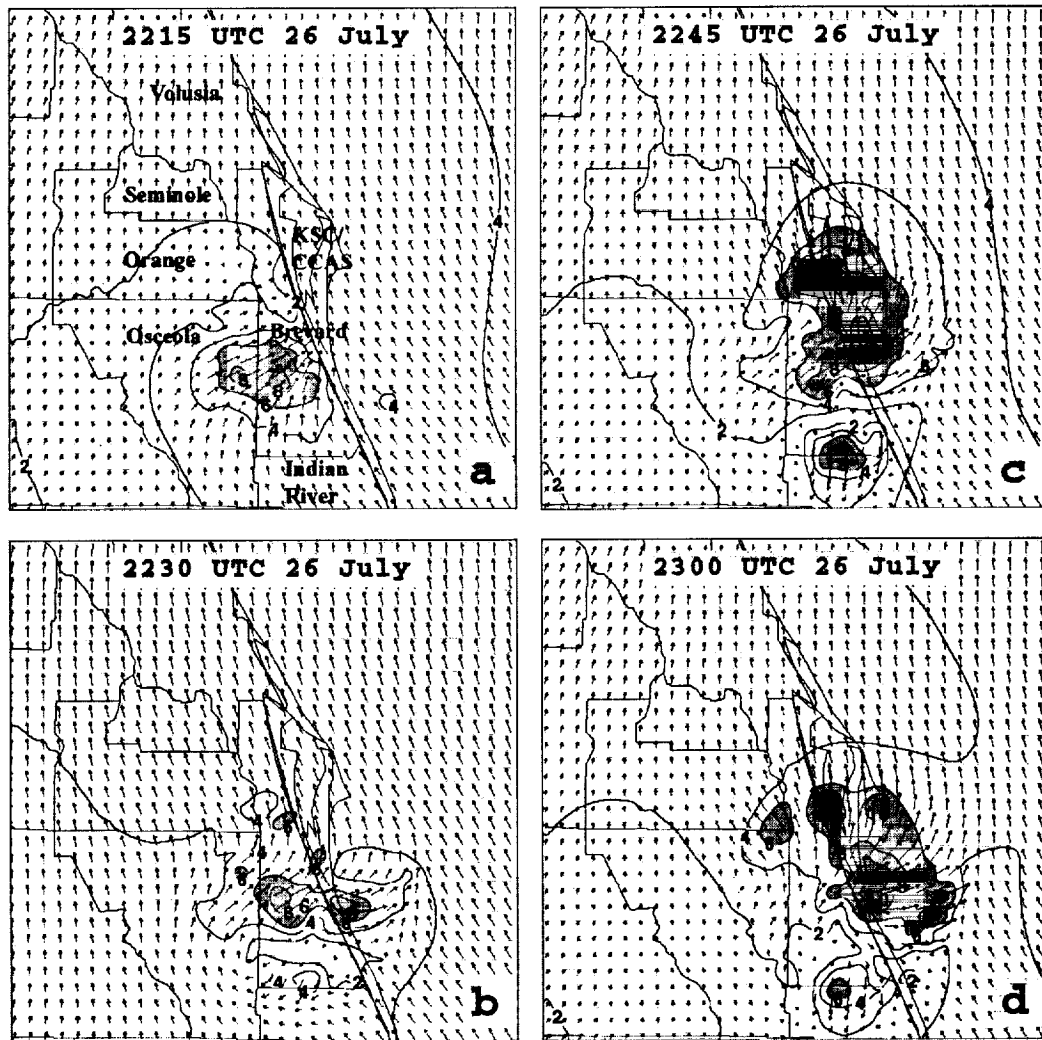


Figure 2. A display of the 2-km ADAS wind speed and wind vectors at 480 m. Wind speed is contoured every 2 m s^{-1} , shaded above 6 m s^{-1} , while wind vectors are denoted by arrows. Valid times are a) 2215 UTC, b) 2230 UTC, c) 2245 UTC, and d) 2300 UTC 26 July. Counties and the location of KSC/CCAS are labeled in a).

Notice that the low-level convergence slopes upward from near the surface in the middle of Figure 4c to 500 m at the north/south (left/right) edges. This structure results from the incorporation of WSR-88D radial velocity data which slopes upward away from the radar site located approximately in the middle of the cross section. Above 200 m, surface data do not influence the analyses. Therefore, changes in the horizontal winds and corresponding divergence field above the surface develop primarily in response to WSR-88D radial velocities in areas where radar reflectivity targets are available.

Finally, the vertical structure of the kinematically-derived vertical velocity field associated with the dissipating convection is depicted in Figure 5. Also shown in Figure 5 is the evolution of the derived circulation (arrows) in the plane of the cross section. At 2215 UTC, a strong updraft greater than 200 cm s^{-1} occurs above 5500 m (Fig. 5a) in conjunction with the deep column of convergence in Figure 4a. Rising motion prevails throughout much of the depth of the

convective cell with values of w exceeding 10 cm s^{-1} from 750 m up to the top of the cross section. Also, a southerly wind component prevails across the southern (right) half of Figure 5a (most notably below 3000 m) which feeds the updraft of the storm.

During the transition phase of the thunderstorm, an area of sinking motion is indicated in the lowest 2-3 km beneath the still strong updraft (Fig 5b). Notice that the prevailing southerly wind component has weakened below 1000 m in the southern (right) portion of Figure 5b. By 2245 UTC, a significant but narrow downdraft has developed from near the surface up to 6000 m between two updrafts (Fig. 5c). Sinking motion reaches 75 cm s^{-1} by this time at roughly 3500 m. In the lowest 1000 m of Figure 5c, southerlies increase in intensity to the north (left) of the strengthening downdraft whereas winds have turned around to a slight northerly component below 1000 m to the south (right) of the downdraft.

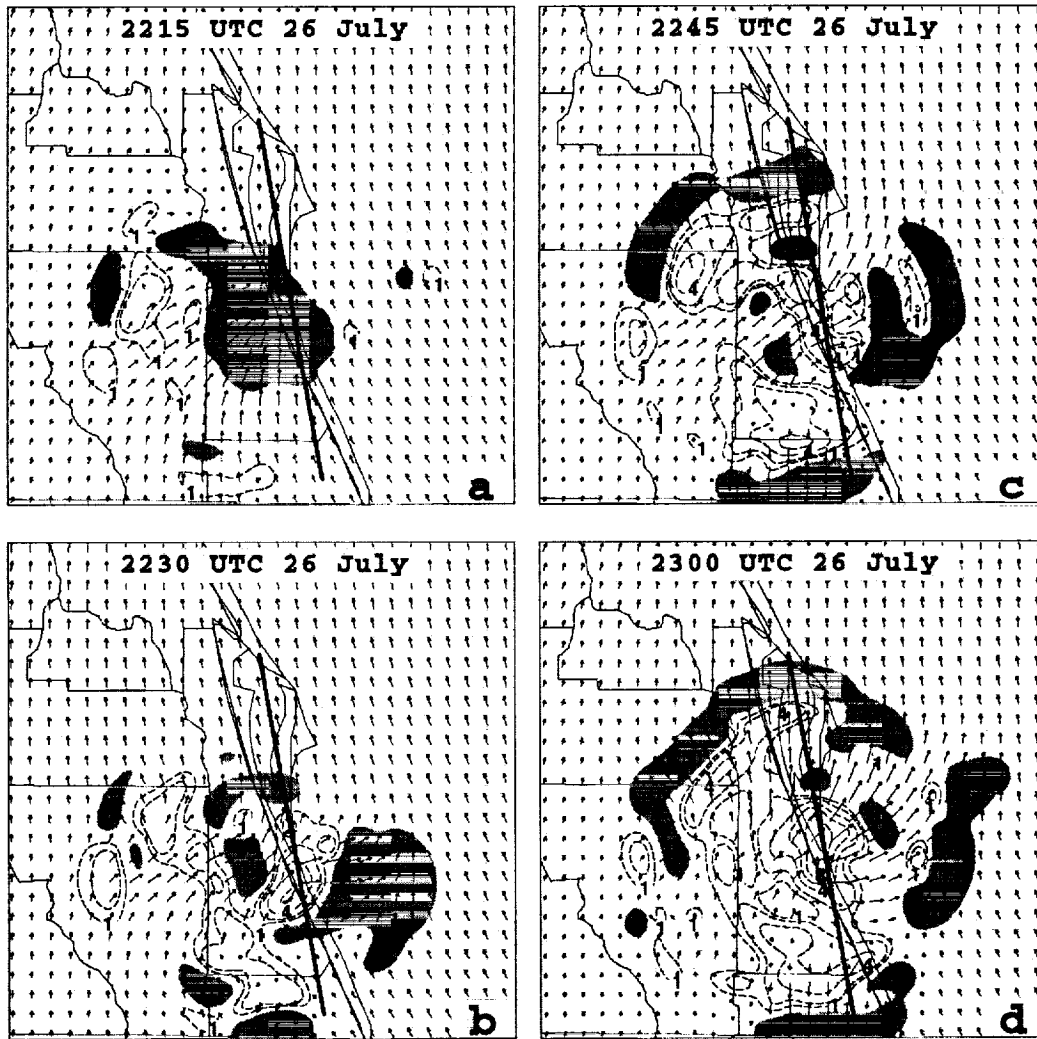


Figure 3. Divergence of the horizontal wind ($\times 10^4 \text{ s}^{-1}$) and wind vectors at 650 m derived from the 2-km ADAS grids. Dashed lines indicate divergence and shading indicates convergence. Valid times are a) 2215 UTC, b) 2230 UTC, c) 2245 UTC, and d) 2300 UTC 26 July.

The mature phase of the outflow boundary at 2300 UTC features a massive downdraft in the center of Figure 5d. The circulation vectors indicate that as the downdraft nears the surface (below 1000 m), the wind strongly diverges and spreads laterally just above the ground resulting in strong southerlies to the north (left) of the downdraft and a northerly wind component to the south (right) of the main downdraft.

It is interesting to note that southerlies prevail below 1000 m over the length of the cross section at 2215 UTC (Fig. 5a). However, the outflow boundary acts to strengthen the low-level southerlies to the north (left) of the downdraft while the southerlies weaken and turn to northerlies to the south (right) of the downdraft by 2300 UTC (Fig. 5d).

For the methodology used in this case, the analyzed thermodynamic variables are not consistent with the derived kinematic fields (i.e. no cold pool is analyzed in the vicinity of the strong thunderstorm downdraft). However, a more sophisticated technique is available within ADAS to retrieve the three-dimensional temperature and pressure distributions from Doppler radar data. This scheme provides more representative analyses of mass and wind fields associated

with mesoscale phenomena that can be used to initialize numerical weather prediction models.

5. SUMMARY

Results from the 26-27 July 1997 case demonstrate that subsequent 15-min analyses of horizontal winds and its associated divergence and derived vertical motion fields on the 2-km ADAS domain can depict the formation and propagation of a thunderstorm outflow boundary. LDIS has the potential to provide added value because it can incorporate data which are currently available only at KSC/CCAS and run at finer spatial and temporal resolutions over smaller domains than current national-scale, operational models such as the RUC and Eta. Furthermore, it is noticeably easier to diagnose and visualize the vertical motion fields and outflow boundary using ADAS analyses rather than strictly radial velocity data at multiple elevation angles.

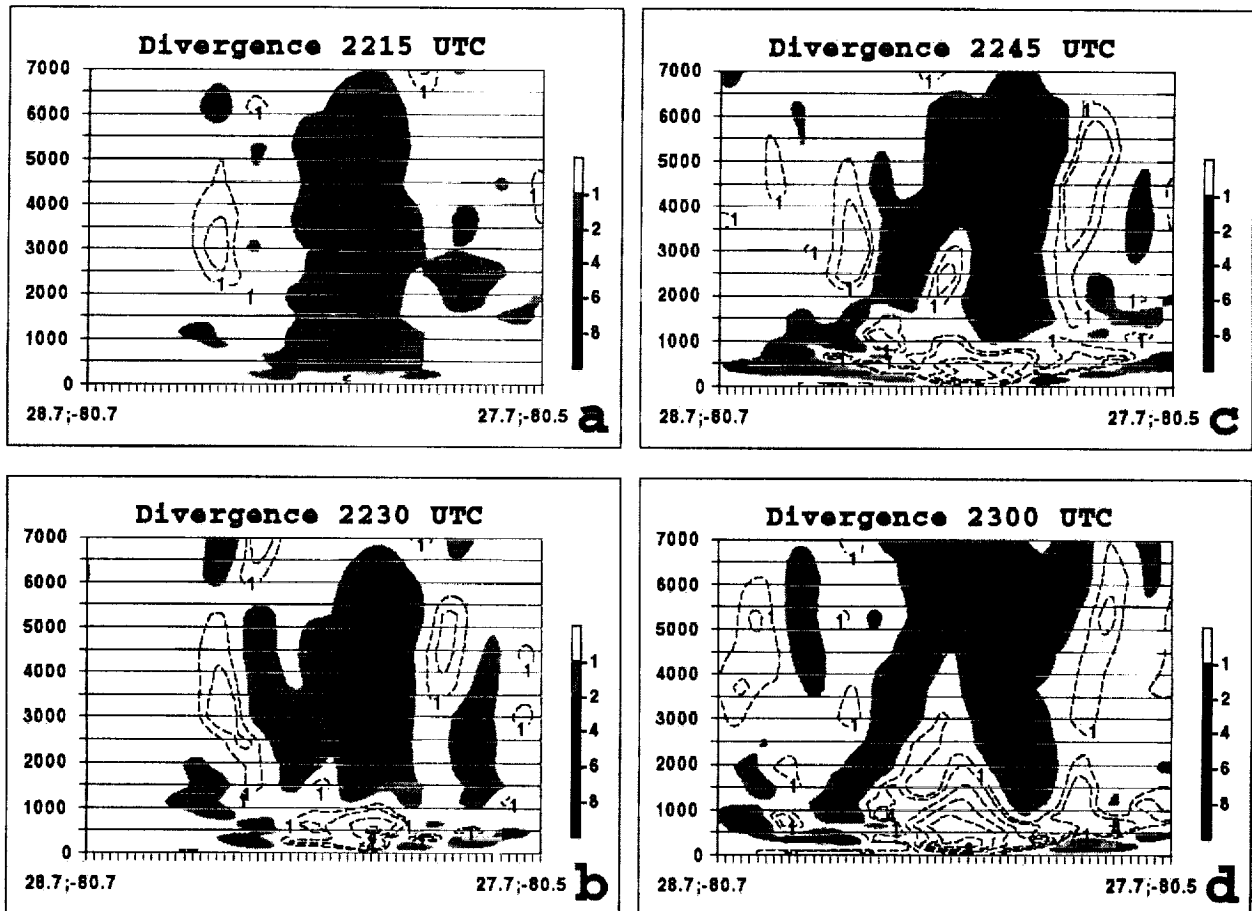


Figure 4. Cross sections of divergence of the horizontal wind ($\times 10^4 \text{ s}^{-1}$, derived from the 2-km ADAS grids) along north-south oriented lines indicated in Figure 3. Dashed lines indicate divergence while shading represents convergence according to the scale provided. Valid times are a) 2215 UTC, b) 2230 UTC, c) 2245 UTC, and d) 2300 UTC 26 July. The ordinate ranges from 0 to 7000 m whereas the latitude and longitude are labeled at the endpoints of the abscissa.

6. REFERENCES

- Benjamin, S. G., J. M. Brown, K. J. Brundage, D. Devenyi, B. E. Schwartz, T. G. Smirnova, T. L. Smith, L. L. Morone, and G. J. DiMego, 1998: The operational RUC-2. *16th Conf. on Weather Analysis and Forecasting*, Phoenix, AZ, Amer. Meteor. Soc., 249-252.
- Berghorsson, P., and B. Doos, 1955: Numerical weather map analysis. *Tellus*, **7**, 329-340.
- Bratseth, A. M., 1986: Statistical interpolation by means of successive corrections. *Tellus*, **38A**, 439-447.
- Brewster, K., 1996: Application of a Bratseth analysis scheme including Doppler radar data. Preprints, *15th Conf. on Weather Analysis and Forecasting*, Norfolk, VA, Amer. Meteor. Soc., 92-95.
- Carr, F. H., J. M. Krause, and K. Brewster, 1996: Application of the Bratseth scheme to high-resolution analyses in inhomogeneous data regimes. Preprints, *15th Conf. on Weather Analysis and Forecasting*, Norfolk, VA, Amer. Meteor. Soc., 231-234.
- Cole, R. E., and W. W. Wilson, 1995: ITWS gridded winds product. Preprints, *6th Conf. on Aviation Weather Systems*, Dallas, TX, Amer. Meteor. Soc., 384-388.
- Manobianco, J. and P. Nutter, 1998: A local data integration system configured for weather support in east central Florida. Preprints, *2nd Symp. on Integrated Observing Systems*, Phoenix, AZ, Amer. Meteor. Soc., 64-67.

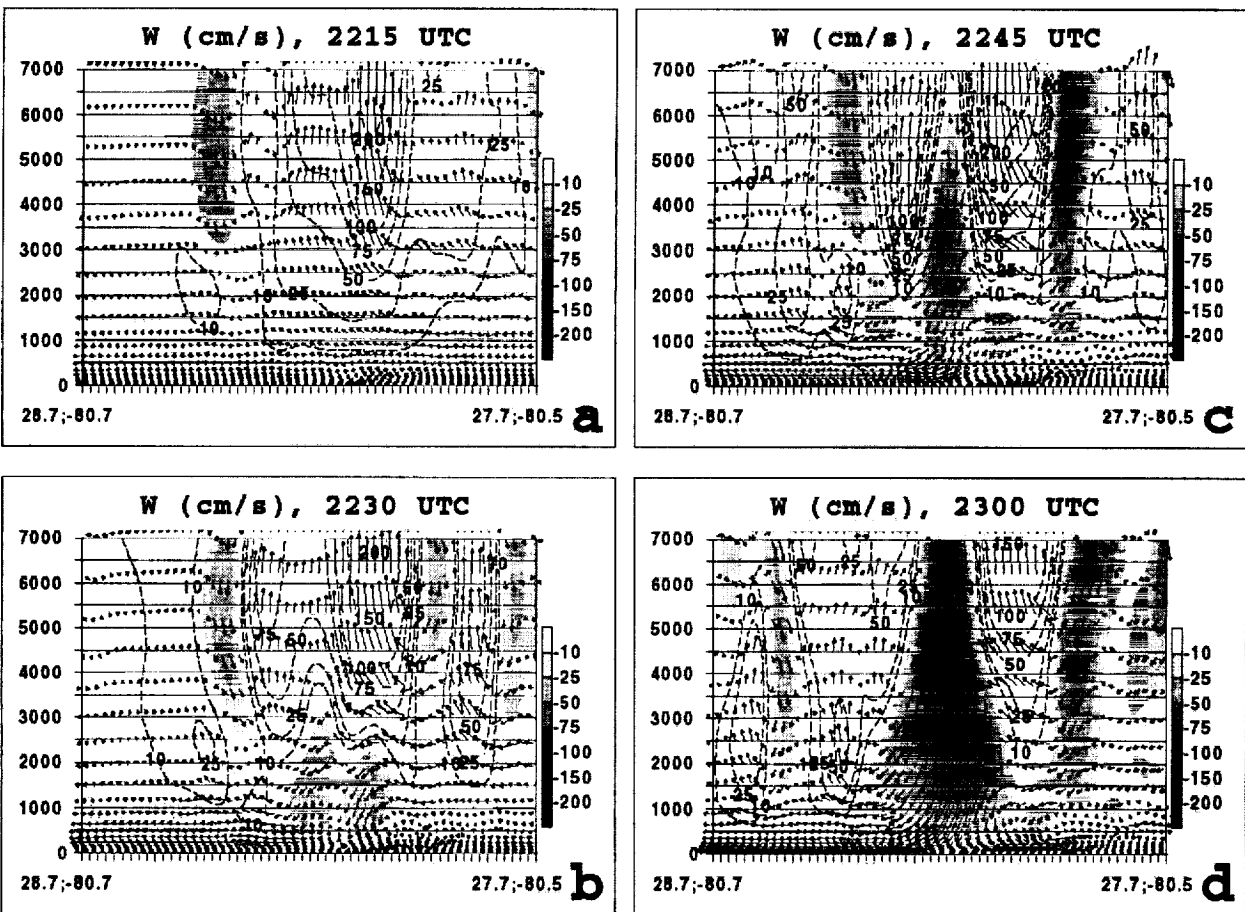


Figure 5. Cross sections of vertical velocity (cm s^{-1} , derived from the 2-km ADAS grids) along north-south oriented lines indicated in Figure 3. Dashed lines indicate rising motion whereas shading represents sinking motion according to the scale provided. Valid times are a) 2215 UTC, b) 2230 UTC, c) 2245 UTC, and d) 2300 UTC 26 July. The ordinate ranges from 0 to 7000 m whereas the latitude and longitude are labeled at the endpoints of the abscissa.

LOCAL DATA INTEGRATION IN EAST CENTRAL FLORIDA

Jonathan L. Case* and John T. Manobianco
 NASA Kennedy Space Center / Applied Meteorology Unit / ENSCO, Inc.
 1980 N. Atlantic Ave. Suite 230
 Cocoa Beach, FL 32931

1. INTRODUCTION

The Applied Meteorology Unit has configured a Local Data Integration System (LDIS) for east central Florida which assimilates in-situ and remotely-sensed observational data into a series of high-resolution gridded analyses. The ultimate goal for running LDIS is to generate products that may enhance weather nowcasts and short-range (< 6 h) forecasts issued in support of the 45th Weather Squadron (45 WS), Spaceflight Meteorology Group (SMG), and the Melbourne National Weather Service (NWS MLB) operational requirements.

LDIS has the potential to provide added value for nowcasts and short-term forecasts for two reasons. First, it incorporates all data operationally available in east central Florida. Second, it is run at finer spatial and temporal resolutions than current national-scale operational models such as the Rapid Update Cycle (RUC; Benjamin et al. 1998) and Eta models. LDIS combines all available data to produce grid analyses of primary variables (wind, temperature, etc.) at specified temporal and spatial resolutions. These analyses of primary variables can be used to compute diagnostic quantities such as vorticity and divergence.

This paper demonstrates the utility of LDIS over east central Florida for a warm season case study. The evolution of a significant thunderstorm outflow boundary is depicted through horizontal and vertical cross section plots of wind speed, divergence, and circulation. In combination with a suitable visualization tool, LDIS may provide users with a more complete and comprehensive understanding of evolving mesoscale weather than could be developed by individually examining the disparate data sets over the same area and time.

2. DATA COVERAGE AND RESOLUTION

The utility of LDIS depends to a large extent on the reliability and availability of both in-situ and remotely-sensed observational data. Therefore, it is important to document all existing meteorological data sources around central Florida that can be incorporated by LDIS.

Data density and coverage in east central Florida vary considerably depending on the level in the atmosphere and distance from KSC/CCAS. The data that are currently incorporated into LDIS include surface, buoy, ship, Kennedy Space Center/Cape Canaveral Air Station (KSC/CCAS) tower and wind profiler, GOES-8, WSR-88D, rawinsonde, and commercial aircraft observations. The data sources that contain the finest horizontal resolution are WSR-88D (< 1 km), GOES-8 visible and infrared imagery (1 km and

4 km), and KSC/CCAS tower observations (4 km). The greatest frequency of observations are provided by WSR-88D, KSC/CCAS towers, profilers, ACARS (Aeronautical Radio, Inc. [ARINC] Communications, Addressing, and Reporting System), and GOES-8 satellite imagery (≤ 15 minutes). The largest variability in horizontal/vertical coverage and density occurs with aircraft data, satellite soundings, and satellite-derived winds. The maximum density of near-surface wind and temperature observations occurs within KSC/CCAS as a result of the tower network. Manobianco and Nutter (1998) provide further details on the data distribution, coverage, and resolution used for this specific configuration of LDIS.

3. ANALYSIS CONFIGURATION

The software utilized for LDIS is the Advanced Regional Prediction System (ARPS) Data Analysis System (ADAS; Brewster 1996; Carr et al. 1996) available from the University of Oklahoma. The analyses in ADAS are produced following Bratseth (1986) who developed an iterative Successive Corrections Method (SCM; Bergthorsson and Doos 1955) that converges to statistical or optimum interpolation (OI). In general, OI schemes are superior to SCM methods because they can account for variations in data density, errors in the data, and dynamical relationships between variables such as the wind components and pressure.

The configuration of ADAS follows the layout used for the terminal wind analysis in the Integrated Terminal Weather System (ITWS; Cole and Wilson 1995). ADAS is run every 15 minutes at 0, 15, 30, and 45 minutes past the hour, over outer and inner grids with horizontal resolutions of 10 km and 2 km, respectively. The 10-km (2-km) analysis domain covers an area of 500 \times 500 km (200 \times 200 km) and consists of 30 vertical levels that extend from the surface to about 16.5 km above ground level. The vertical levels are stretched, with the finest resolution near the surface (20 m spacing) and the coarsest resolution at upper levels (~1.8 km spacing).

The background fields used on the 10-km analysis domain are the RUC grids of temperature, wind, relative humidity, and geopotential height at 25-mb intervals from 1000 to 100 mb. The RUC analyses are available at a horizontal resolution of 60-km every 3-h for the case study presented in this paper. The RUC grids are linearly interpolated in time every 15 minutes for each 10-km ADAS cycle. The resulting 10-km analysis grids are then used as background fields for analyses on the 2-km domain. This nested-grid configuration and cascade-of-scales analysis follows that used for terminal winds in ITWS. With such an approach, it is possible to analyze for different temporal and spatial scales of weather phenomena.

The observational data are incorporated into ADAS using multiple passes of the Bratseth scheme to account for the varying spatial resolution of the data sources. Five

*Corresponding author address: Jonathan Case, ENSCO, Inc., 1980 N. Atlantic Ave., Suite 230, Cocoa Beach, FL 32931. E-mail: jonc@fl.ensco.com.

computational passes are used for the 10-km grid and four passes are utilized on the 2-km grid. Data with similar resolutions are grouped together in the same computational pass such that ADAS incorporates each data source without excessively smoothing the resolvable meteorological features. This methodology ensures that each data source is utilized in ADAS to its maximum potential based on the meteorological features that the data can resolve.

4. DIAGNOSIS OF AN OUTFLOW BOUNDARY

A warm season case was selected from 26-27 July 1997 in order to investigate the capabilities and utility provided by ADAS. Both 10-km and 2-km grid analyses were generated for the warm season case at 15-minute intervals from 1800 UTC 26 July to 0200 UTC 27 July using all available data. However, only results from the 2-km analysis grid are presented in this section.

A typical, undisturbed warm season environment characterized the 26-27 July 1997 case. Early in the afternoon, scattered thunderstorms developed across the peninsula and a sea-breeze boundary was evident along the east coast (not shown). By 2212 UTC, strong thunderstorms developed southwest of KSC/CCAS and generated an outflow boundary that propagated northeastward as indicated by the Melbourne WSR-88D level II base reflectivity (Fig. 1a). The leading edge of the outflow boundary intersected the eastern tip of KSC/CCAS by 2242 UTC as shown in Figure 1b (counties and location of KSC/CCAS are given in Fig. 2a). This outflow boundary caused wind gusts greater than 15 m s^{-1} as noted on the KSC/CCAS mesonet towers around 2245 UTC (not shown). This case was chosen because the strong winds associated with the outflow boundary forced Atlas launch operation A1393 to be scrubbed for the day.

Using the fine-scale results of the 2-km ADAS analyses, the evolution of the wind speeds and wind vectors at 480 m (Figs. 2a-d) illustrates the formation and intensification of the outflow boundary during the late afternoon of 26 July. Wind speeds greater than 8 m s^{-1} develop over the Brevard/Osceola county border at 2215 UTC 26 July (Fig. 2a) and spread radially over the next 45 minutes. The maximum winds ($> 12 \text{ m s}^{-1}$) move northeastward into KSC/CCAS and offshore regions of central Brevard county by 2245 UTC (Fig. 3c), the approximate time that the Atlas launch was postponed.

Examination of level II radar reflectivity (Fig. 1) and radial velocity data (not shown) indicates that features present in the high-resolution wind analyses (Fig. 2) are consistent with the scale and motion of patterns associated with the observed thunderstorm. It should be noted that the detailed structure of horizontal winds associated with this outflow boundary would likely be easier to visualize in real-time using ADAS rather than WSR-88D radial velocity displays alone.

The evolution of the thunderstorm outflow can also be examined through the divergence of the horizontal wind on the 2-km ADAS grid. In Figure 3, plots of convergence (shaded), divergence (dashed lines), and horizontal winds are shown at 650 m for the same times as in Figure 2. At 2215 UTC, an area of low-level convergence is found over much of central Brevard county (Fig. 3a). Weak divergence is also found over northeastern Osceola county at this time. Fifteen minutes later, an extensive area of low-level divergence develops in southern Brevard county, behind the developing outflow boundary (Fig. 3b). Convergence along the outflow boundary spreads outward into central Brevard county (just south of KSC/CCAS), offshore of southern Brevard county, and into Indian River county. Divergence continues to intensify across much of interior Brevard county over the next 30 minutes beneath the dissipating thunderstorm (Figs. 3c and d), while the band of convergence spreads out radially along the leading edge of the outflow boundary.

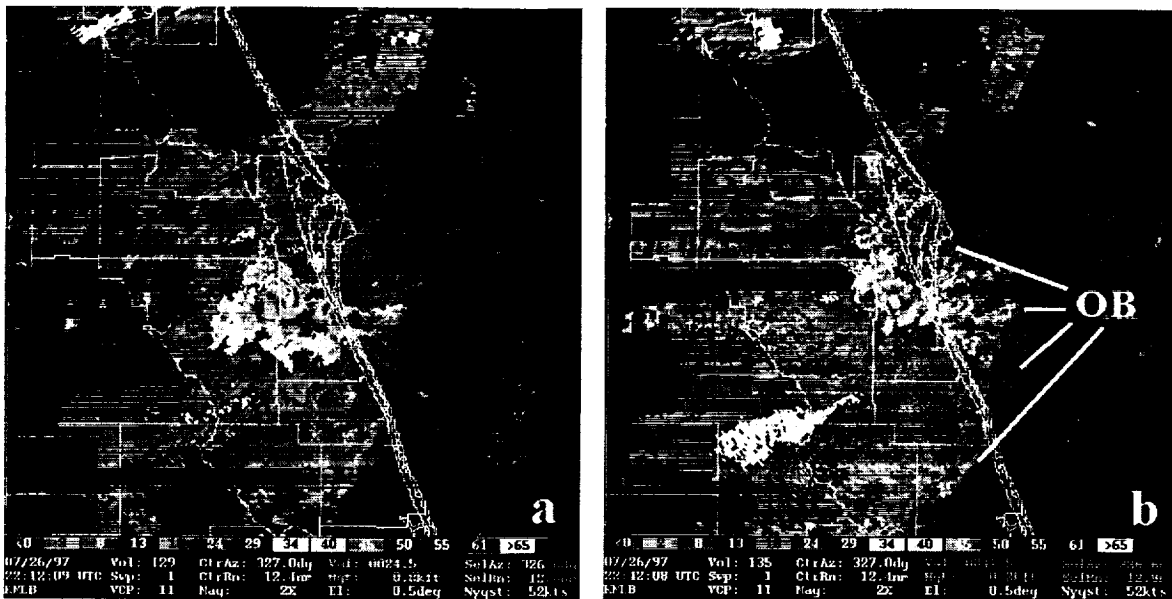


Figure 1. Base reflectivity images are shown from the Melbourne WSR-88D on 26 July at a) 2212 UTC and b) 2242 UTC. The leading edge of the outflow boundary is indicated by "OB" in panel b).

By 2300 UTC, a well-defined band of convergence arcs from northern Osceola county, across eastern Orange and northern Brevard county, into the offshore waters of Brevard county, and then back onshore in Indian River county (Fig. 3d). Strong divergence exceeding $8 \times 10^{-4} \text{ s}^{-1}$ occurs over east-central Brevard county.

The vertical structure of the convection is indicated by north-south cross sections of divergence and the vertical velocity (w) field through the developing thunderstorm outflow (Fig. 4 and 5 respectively). According to Brewster (1996), w is derived within ADAS from the analyzed horizontal winds (via continuity) and a constraint that the wind velocity normal to the bottom and top boundaries is zero. Deviations from these boundary conditions are treated as errors in the horizontal divergence that vary linearly with height. The w field is adjusted once these errors are removed and the horizontal wind field is relaxed such that total mass divergence domain-wide is zero.

A deep column of convergence is prevalent at 2215 UTC (Fig. 4a) associated with the strong convection southwest of

KSC/CCAS (Fig. 1a). The onset of the dissipating stage of the convection occurs at 2230 UTC when convergence transitions to divergence in the lowest 1000 m directly beneath the deep layer of maximum convergence (Fig. 4b). The leading edge of the outflow boundary is evident in Figure 4b given by the low-level convergence below 1000 m on either side of the newly-developed low-level divergence.

By 2245 UTC, the area of low-level divergence expands laterally and upward to 3000 m (Fig. 4c). The leading edge of the outflow boundary spreads rapidly north and southward (left and right, primarily below 1000 m) on either side of the intensifying low-level divergence maximum. Meanwhile, mid-level convergence remains strong, exceeding $-6 \times 10^{-4} \text{ s}^{-1}$ in the 3500–5500-m layer. By 2300 UTC, a well-developed signature exists for a downburst-producing thunderstorm (Fig. 4d). Strong mid-level convergence in the 3000–6000-m layer overlies a maximum in low-level divergence which exceeds $8 \times 10^{-4} \text{ s}^{-1}$.

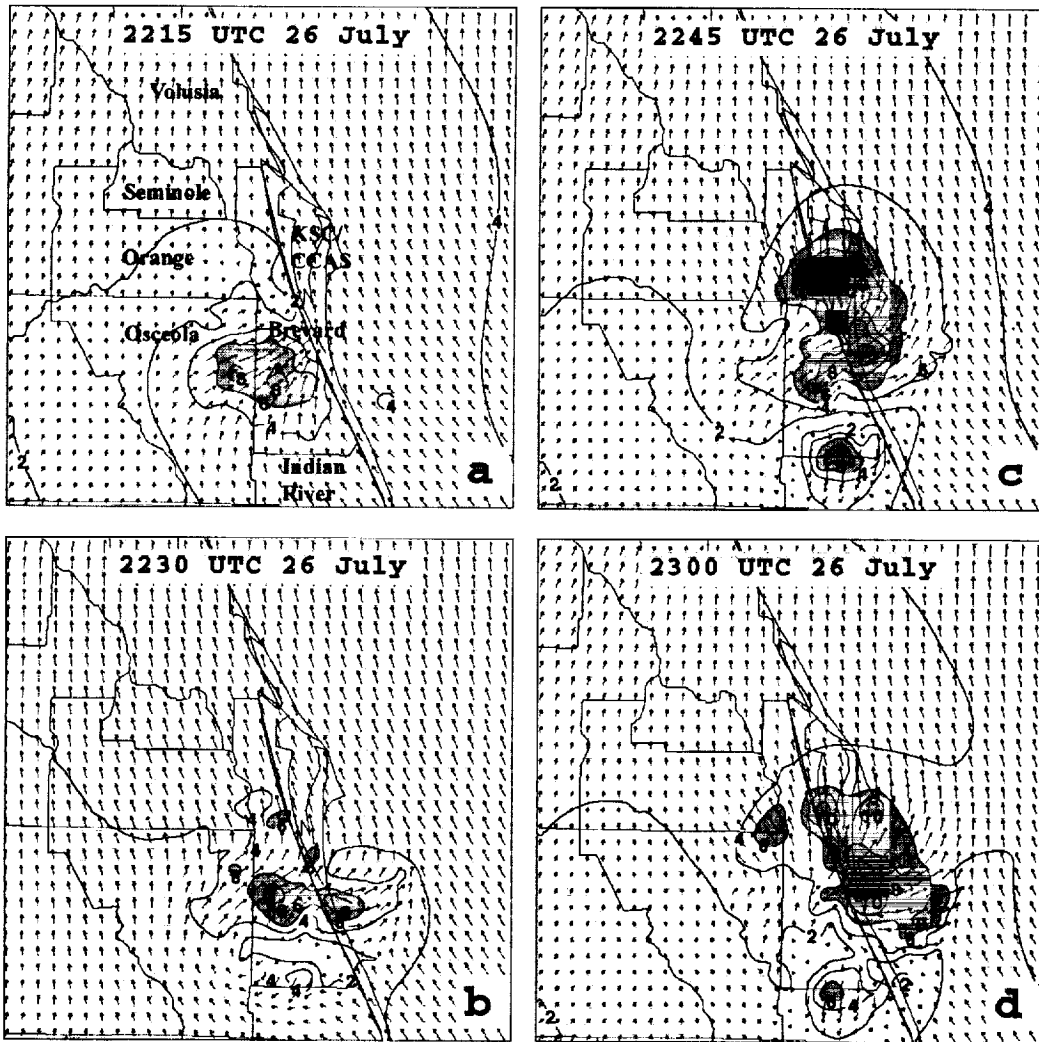


Figure 2. A display of the 2-km ADAS wind speed and wind vectors at 480 m. Wind speed is contoured every 2 m s^{-1} , shaded above 6 m s^{-1} , while wind vectors are denoted by arrows. Valid times are a) 2215 UTC, b) 2230 UTC, c) 2245 UTC, and d) 2300 UTC 26 July. Counties and the location of KSC/CCAS are labeled in a).

Notice that the low-level convergence slopes upward from near the surface in the middle of Figure 4c to 500 m at the north/south (left/right) edges. This structure results from the incorporation of WSR-88D radial velocity data which slopes upward away from the radar site located approximately in the middle of the cross section. Above 200 m, surface data do not influence the analyses. Therefore, changes in the horizontal winds and corresponding divergence field above the surface develop primarily in response to WSR-88D radial velocities in areas where radar reflectivity targets are available.

Finally, the vertical structure of the kinematically-derived vertical velocity field associated with the dissipating convection is depicted in Figure 5. Also shown in Figure 5 is the evolution of the derived circulation (arrows) in the plane of the cross section. At 2215 UTC, a strong updraft greater than 200 cm s^{-1} occurs above 5500 m (Fig. 5a) in conjunction with the deep column of convergence in Figure 4a. Rising motion prevails throughout much of the depth of the

convective cell with values of w exceeding 10 cm s^{-1} from 750 m up to the top of the cross section. Also, a southerly wind component prevails across the southern (right) half of Figure 5a (most notably below 3000 m) which feeds the updraft of the storm.

During the transition phase of the thunderstorm, an area of sinking motion is indicated in the lowest 2-3 km beneath the still strong updraft (Fig 5b). Notice that the prevailing southerly wind component has weakened below 1000 m in the southern (right) portion of Figure 5b. By 2245 UTC, a significant but narrow downdraft has developed from near the surface up to 6000 m between two updrafts (Fig. 5c). Sinking motion reaches 75 cm s^{-1} by this time at roughly 3500 m. In the lowest 1000 m of Figure 5c, southerlies increase in intensity to the north (left) of the strengthening downdraft whereas winds have turned around to a slight northerly component below 1000 m to the south (right) of the downdraft.

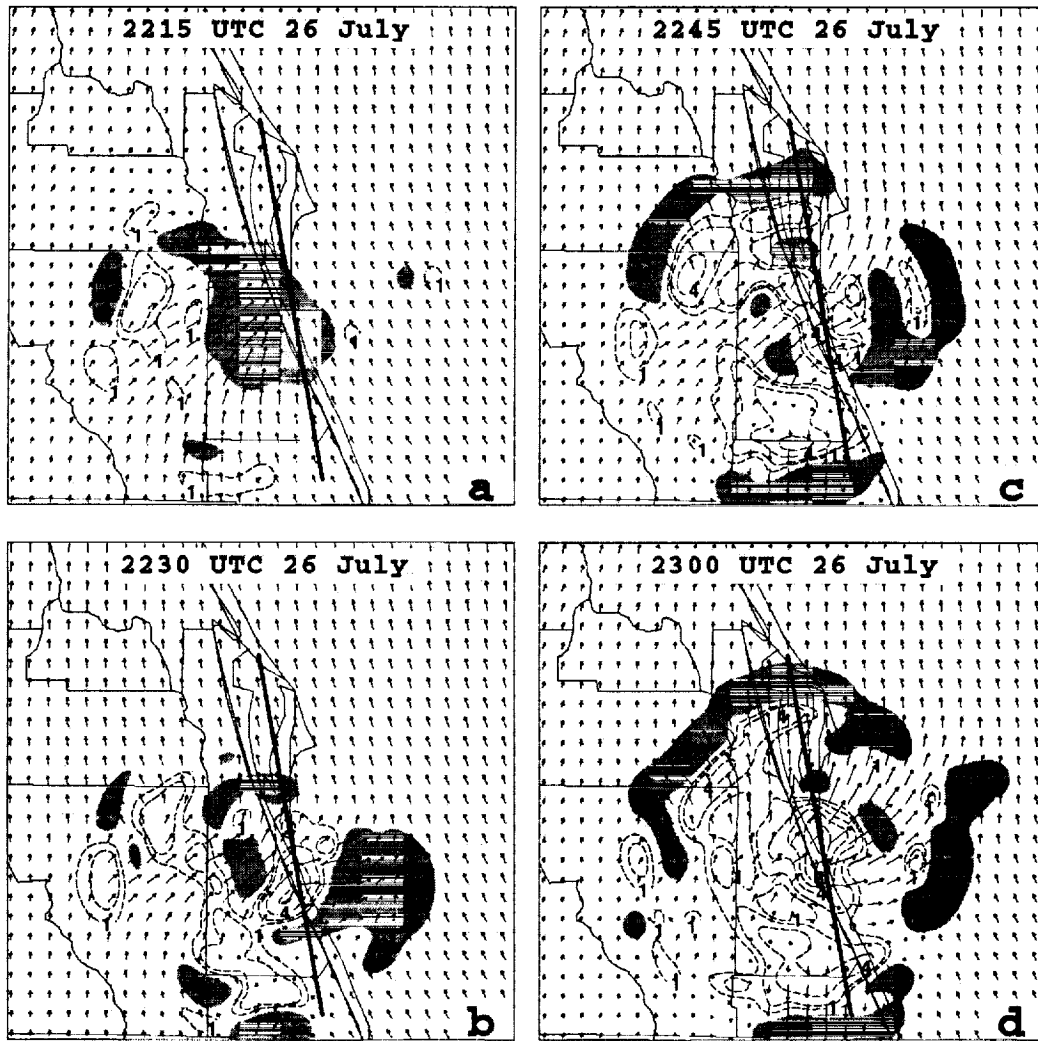


Figure 3. Divergence of the horizontal wind ($\times 10^4 \text{ s}^{-1}$) and wind vectors at 650 m derived from the 2-km ADAS grids. Dashed lines indicate divergence and shading indicates convergence. Valid times are a) 2215 UTC, b) 2230 UTC, c) 2245 UTC, and d) 2300 UTC 26 July.

The mature phase of the outflow boundary at 2300 UTC features a massive downdraft in the center of Figure 5d. The circulation vectors indicate that as the downdraft nears the surface (below 1000 m), the wind strongly diverges and spreads laterally just above the ground resulting in strong southerlies to the north (left) of the downdraft and a northerly wind component to the south (right) of the main downdraft.

It is interesting to note that southerlies prevail below 1000 m over the length of the cross section at 2215 UTC (Fig. 5a). However, the outflow boundary acts to strengthen the low-level southerlies to the north (left) of the downdraft while the southerlies weaken and turn to northerlies to the south (right) of the downdraft by 2300 UTC (Fig. 5d).

For the methodology used in this case, the analyzed thermodynamic variables are not consistent with the derived kinematic fields (i.e. no cold pool is analyzed in the vicinity of the strong thunderstorm downdraft). However, a more sophisticated technique is available within ADAS to retrieve the three-dimensional temperature and pressure distributions from Doppler radar data. This scheme provides more representative analyses of mass and wind fields associated

with mesoscale phenomena that can be used to initialize numerical weather prediction models.

5. SUMMARY

Results from the 26-27 July 1997 case demonstrate that subsequent 15-min analyses of horizontal winds and its associated divergence and derived vertical motion fields on the 2-km ADAS domain can depict the formation and propagation of a thunderstorm outflow boundary. LDIS has the potential to provide added value because it can incorporate data which are currently available only at KSC/CCAS and run at finer spatial and temporal resolutions over smaller domains than current national-scale, operational models such as the RUC and Eta. Furthermore, it is noticeably easier to diagnose and visualize the vertical motion fields and outflow boundary using ADAS analyses rather than strictly radial velocity data at multiple elevation angles.

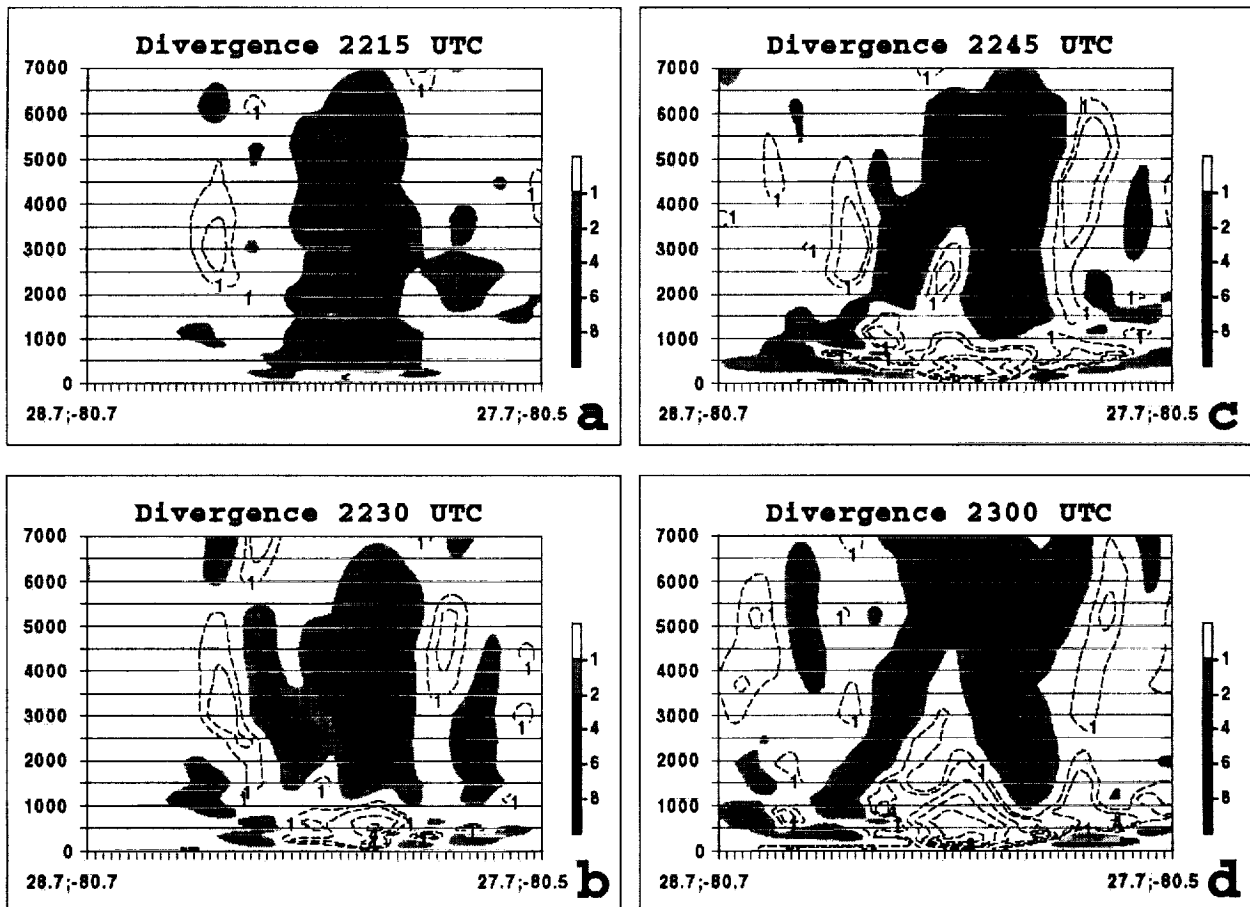


Figure 4. Cross sections of divergence of the horizontal wind ($\times 10^{-4} \text{ s}^{-1}$, derived from the 2-km ADAS grids) along north-south oriented lines indicated in Figure 3. Dashed lines indicate divergence while shading represents convergence according to the scale provided. Valid times are a) 2215 UTC, b) 2230 UTC, c) 2245 UTC, and d) 2300 UTC 26 July. The ordinate ranges from 0 to 7000 m whereas the latitude and longitude are labeled at the endpoints of the abscissa.

6. REFERENCES

- Benjamin, S. G., J. M. Brown, K. J. Brundage, D. Devenyi, B. E. Schwartz, T. G. Smirnova, T. L. Smith, L. L. Morone, and G. J. DiMego, 1998: The operational RUC-2. *16th Conf. on Weather Analysis and Forecasting*, Phoenix, AZ, Amer. Meteor. Soc., 249-252.
- Bergthorsson, P., and B. Doos, 1955: Numerical weather map analysis. *Tellus*, 7, 329-340.
- Bratseth, A. M., 1986: Statistical interpolation by means of successive corrections. *Tellus*, 38A, 439-447.
- Brewster, K., 1996: Application of a Bratseth analysis scheme including Doppler radar data. Preprints, *15th Conf. on Weather Analysis and Forecasting*, Norfolk, VA, Amer. Meteor. Soc., 92-95.
- Carr, F. H., J. M. Krause, and K. Brewster, 1996: Application of the Bratseth scheme to high-resolution analyses in inhomogeneous data regimes. Preprints, *15th Conf. on Weather Analysis and Forecasting*, Norfolk, VA, Amer. Meteor. Soc., 231-234.
- Cole, R. E., and W. W. Wilson, 1995: ITWS gridded winds product. Preprints, *6th Conf. on Aviation Weather Systems*, Dallas, TX, Amer. Meteor. Soc., 384-388.
- Manobianco, J. and P. Nutter, 1998: A local data integration system configured for weather support in east central Florida. Preprints, *2nd Symp. on Integrated Observing Systems*, Phoenix, AZ, Amer. Meteor. Soc., 64-67.

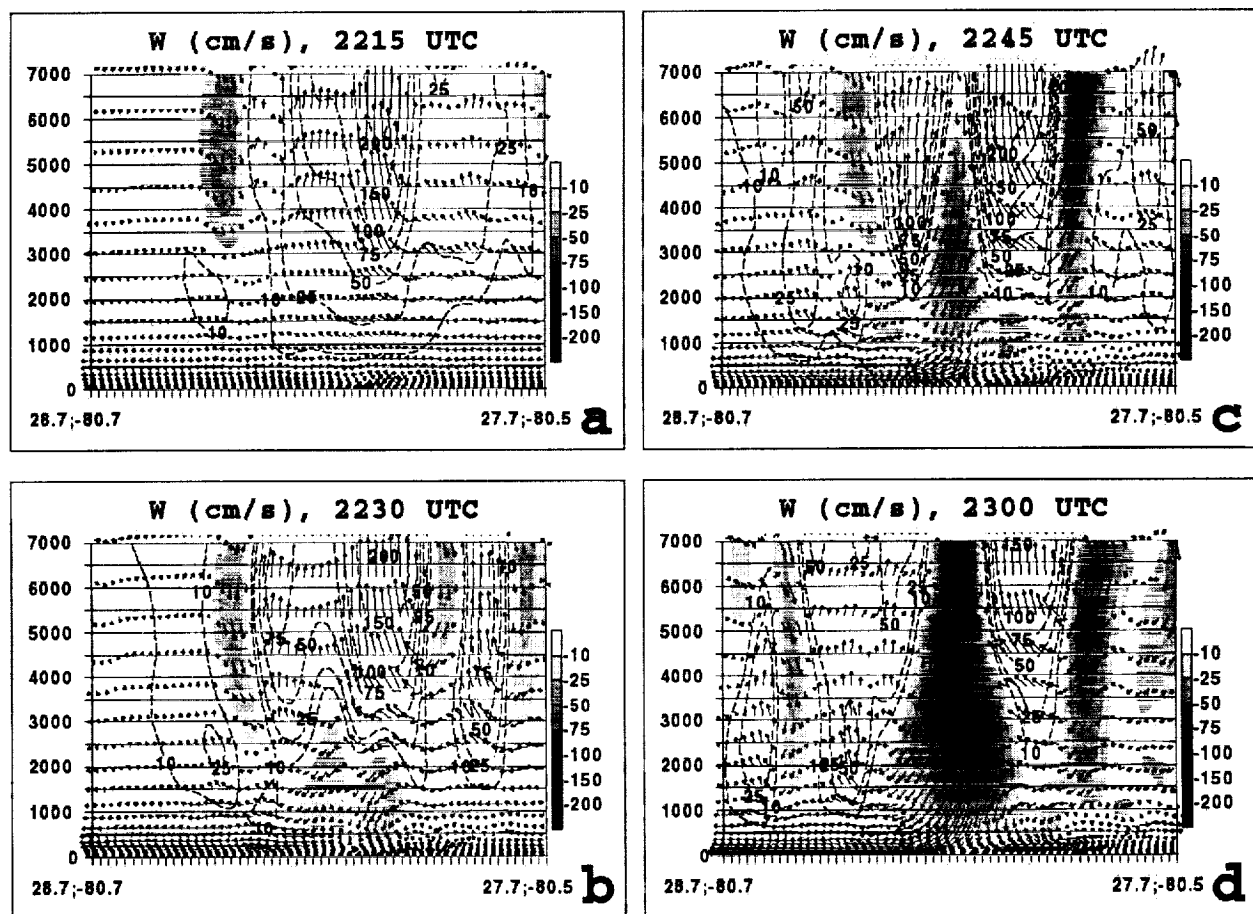


Figure 5. Cross sections of vertical velocity (cm s^{-1} , derived from the 2-km ADAS grids) along north-south oriented lines indicated in Figure 3. Dashed lines indicate rising motion whereas shading represents sinking motion according to the scale provided. Valid times are a) 2215 UTC, b) 2230 UTC, c) 2245 UTC, and d) 2300 UTC 26 July. The ordinate ranges from 0 to 7000 m whereas the latitude and longitude are labeled at the endpoints of the abscissa.